Liquid Crystalline Polyimides. 25. Smectic and Photoreactive Poly(ester—imide)s of 4-Aminocinnamic Acid and α,ω-Dihydroxyalkanes

## Hans R. Kricheldorf,* Nicolas Probst, and Christoph Wutz

Institut für Technische und Makromolekulare Chemie der Universität, Bundesstrasse 45, D-20146 Hamburg, Germany

ABSTRACT: A series of homopoly(ester—imide)s was prepared by polycondensation of α,ω-dihydroxy-alkanes and the dichloride of 4-aminocinnamic acid trimellitimide. Upon moderate or rapid heating and cooling, the poly(ester—imide)s containing odd-numbered spacers form an enantiotropic highly viscous smectic-C phase and the solid state is a frozen smectic-C phase. The longest odd spacer (9 CH_2 groups) enables crystallization upon annealing. All poly(ester—imide)s having even spacers form a monotropic, long-lived smectic liquid crystalline (LC) phase and a quasi-crystalline smectic-H phase in the solid state. The layer distance (*d*-spacing) of the smectic-H phase is considerably shorter than that of the smectic LC phase. The rate of crystallization (formation of the smectic-H phase) increases with the length of the spacer. ^{13}C NMR CP/MAS measurements suggest that the longest aliphatic spacers ($\geq$12, 16, and 22 CH_2 groups) can form an ordered paraffin phase between the "two-dimensional" crystals of the mesogens.

Introduction

Previous studies of several authors[1–8] have demonstrated that poly(ester—imide)s, poly(ether—imide)s, and poly(amide—imide)s built up by a regular sequence of imide mesogens and alkane spacers possess a high tendency to form layer structures in the molten and solid states. The nature of such layer structures and the phase transitions between different layer structures vary largely with the chemical structure of the polyimides. Thus these semialiphatic polyimides are an excellent example for systematic studies of structure—property relationships. For instance, the poly(ester—imide)s of structure **1** have recently attracted some interest, because they can form five different kinds of solid-state phases depending on the length of the spacers and on the thermal history.[4,9] However, the PEI's **1** do not form an enantiotropic liquid crystalline (LC) phase, but only a very short-lived smectic-A phase. The purpose of the present article is to study an analogous class of poly(ester—imide)s (**2**) containing a better mesogen.[10] Furthermore, the PEI's should possess the additional advantage of enabling photo-cross-linking in solution, in the melt, or in the amorphous state.

1(*n* = 4–10,12)

2a–i
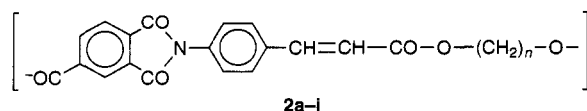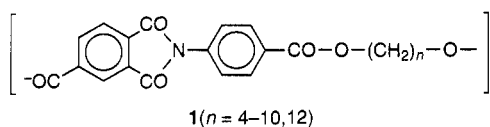
a: *n* = 5	**d**: *n* = 8	**g**: *n* = 12
b: *n* = 6	**e**: *n* = 9	**h**: *n* = 16
c: *n* = 7	**f**: *n* = 10	**i**: *n* = 22

Experimental Section

Materials. Trimellitic anhydride and thionyl chloride were gifts of Bayer AG (Leverkusen, FRG) and were used as

received. *trans*-4-Aminocinnamic acid hydrochloride was purchased from Aldrich (Milwaukee, WI)) and used without further purification. The α,ω-dihydroxyalkanes were also purchased from Aldrich. The shorter ones (*n* ≤ 8) were dried by azeotropic distillation with toluene and distilled in vacuo. The longer ones were dried over P_4O_{10} in vacuo in a desiccator. The *trans*-4 aminocinnamic acid trimellitimide and its dicarboxylic acid chloride (mp 213–215 °C) were prepared as described previously.[9]

Polycondensations. The dichloride of 4-aminocinnamic acid trimellitimide (10 mmol) and α,ω-dihydroxyalkane (10 mmol) were refluxed in dry *o*-dichlorobenzene (15 mL) for 24 h under an atmosphere of nitrogen. After cooling, the reaction mixture was diluted with CH_2Cl_2 (40 mL) and trifluoroacetic acid (5 mL) and precipitated into methanol. The precipitated polyester was isolated by filtration, dried at 80 °C, and reprecipitated from CH_2Cl_2/trifluoroacetic acid (1:1 by volume) into methanol.

Measurements. The inherent viscosities were measured in an automated Ubbelohde viscometer thermostated at 20 °C.

The DSC measurements were conducted with a Perkin-Elmer DSC-4 in aluminum pans under nitrogen.

The 100 MHz ^1H NMR spectra were recorded with a Bruker AC-100 FT-NMR spectrometer in 5 mm o.d. sample tubes.

The WAXD powder patterns were recorded with a Siemens D-500 diffractometer using Ni-filtered Cu Kα radiation. Measurements of the middle-angle reflections were also conducted with synchrotron radiation (λ = 1.50 Å) at a heating and cooling rate of 20 °C/min. The measurements were conducted with a position-sensitive one-dimensional detector in a vacuum oven at HASYLAB, DESY Hamburg.

The UV spectra were recorded with a computer-equipped Cary 5E UV—vis—near-IR spectrophotometer. CH_2Cl_2 solutions with a concentration of *c* = 10^{-5} mol/L were measured in quartz cuvettes with a diameter of 1 cm. All computer simulations were conducted with the force-field program PCFF91 of Biosym's Discover V 2.8.0 program.

Results and Discussion

Syntheses and Characterization. All PEI's of this work were prepared by the same method. The dichloride of *trans*-4-aminocinnamic acid trimellitimide was polycondensed with α,ω-dihydroxyalkanes (eq 1) in *o*-dichlorobenzene as an inert reaction medium. This

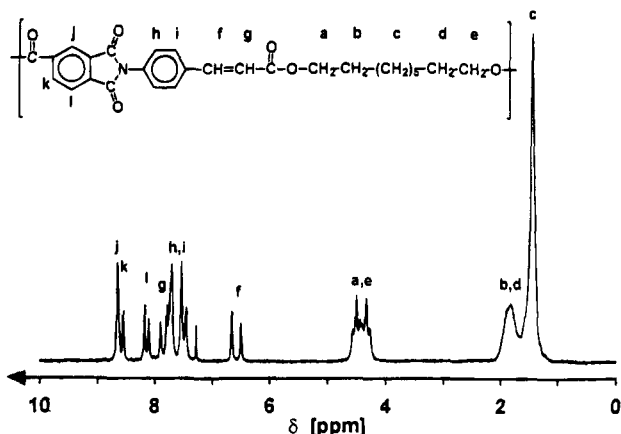$$\xrightarrow{\substack{+HO(CH_2)_nOH \\ -2HCl}} \text{2a–i}$$
(1)
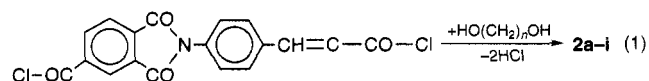
Figure 1. 100 MHz ^{1}H NMR spectrum of poly(ester−imide) **2e** in CDCl$_3$/trifluoroacetic acid (9:1 by volume).

Table 1. Yields and Properties of Poly(ester−imide)s

polymer formula	n	yield (%)	$\eta_{inh}{}^a$ (dL/g)	elem formula (mol wt)		% C	% H	% N
2a	5	84	0.66	C$_{23}$H$_{19}$NO$_6$	calcd	68.14	4.72	3.46
				(405.39)	found	67.41	4.75	3.99
2b	6	91	0.45	C$_{24}$H$_{21}$NO$_6$	calcd	68.72	5.05	3.34
				(419.42)	found	68.54	4.85	3.36
2c	7	81	0.64	C$_{25}$H$_{23}$NO$_6$	calcd	69.27	5.35	3.23
				(433.44)	found	68.30	5.16	2.75
2d	8	92	0.57	C$_{26}$H$_{25}$NO$_6$	calcd	69.78	5.63	3.13
				(447.47)	found	68.89	5.47	2.63
2e	9	91	0.62	C$_{27}$H$_{27}$NO$_6$	calcd	70.26	5.90	3.04
				(461.50)	found	69.36	5.77	2.79
2f	10	99	0.57	C$_{28}$H$_{29}$NO$_6$	calcd	70.72	6.15	2.95
				(475.52)	found	69.83	6.11	2.79
2g	12	89	0.54	C$_{30}$H$_{33}$NO$_6$	calcd	71.55	6.61	2.78
				(503.57)	found	70.87	6.57	2.55
2h	16	93	0.72	C$_{34}$H$_{41}$NO$_6$	calcd	72.96	7.38	2.50
				(559.68)	found	72.24	7.35	2.55
2i	22	70	0.79	C$_{40}$H$_{53}$NO$_6$	calcd	74.62	8.30	2.18
				(643.83)	found	74.02	8.34	1.94

^{a} Measured at 20 °C in CH$_2$Cl$_2$/trifluoroacetic acid (volume ratio 9:1).

liquid was selected because it is an excellent solvent for many polyesters. Furthermore, polycondensations of dicarboxylic acid dichloride and aliphatic diols involve considerable HCl-catalyzed side reaction, such as the formation of ether groups, when conducted in bulk.[6] However, all attempts to obtain PEI's from 1,4-butanediol or 1,3-propanediol failed apparently due to side reactions of the diols. Therefore, PEI's with spacers shorter than 5 CH$_2$ groups were not studied in this work. The chemical structure of all PEI's was examined by ^{1}H NMR spectroscopy, which proved the absence of ether groups and the absence of cis−trans isomerization, as illustrated by Figure 1. The yields, inherent viscosities, and elemental analyses of **2a−i** are compiled in Table 1.

The UV spectroscopic properties of the PEI's need a short comment. When the UV spectrum of PEI **2d** was recorded in CHCl$_3$/trifluoroacetic acid (volume ratio 9:1), an absorption maximum was found at 290 nm. In the case of a thin film, the absorption begins at 380−390 nm and rises sharply around 350 nm. In a couple of preliminary qualitative irradiation experiments, it was found that irradiation of thin films of **2d** or **2g** with light of a wavelength ≤ 360 nm causes cross-linking. More detailed studies of the otpical properties will be published separately.

Properties of PEI's with Odd Spacers. The PEI's **2a, 2c,** and **2e** exhibited a rather uniform behavior with regard to their thermal properties. DSC measurements

Table 2. Thermal Properties of Poly(ester−imide)s 2a−i

polymer formula	n	$T_g{}^a$ (°C)	$T_m{}^a$ (°C)	$\Delta H°_m{}^a$ (kJ/mol)	$T_i{}^b$ (°C)	$T_c{}^c$ (°C)	$\Delta H°_c{}^d$ (kJ/mol)
2a	5	97	149	1.3	152−158		
2b	6	93	223	8.0	225−232	211, 126	−1.0/−3,5
2c	7	79	140	2.5	135−145	121	−2.3
2d	8	78	205	10.0	200−208	189, 137	−1.8/−4.5
2e	9	70	142	3.6	140−145	127	−3.6
2f	10	71	179	13.0	177−180	166, 104	−2.0/−6.5
2g	12	64	167	17.0	165−168	154, 111	−2.5/−7.0
2h	16	69	157	20.0	158−160	139, 120	−5.0/−7.5
2i	22	71	154	23.0	152−155	136.120	−9.0/−11.0

^{a} DSC measurements with a heating rate of 20 °C/min. ^{b} Optical microscopy with a heating rate of 10 °C/min. ^{c} DSC measurements with a cooling rate of −20 °C/min. ^{d} DSC measurements with a cooling rate of −10 °C/min.
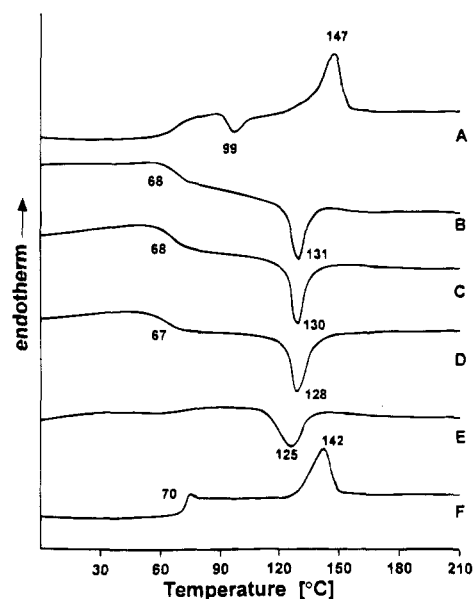

Figure 2. DSC measurements of PEI **2e** (n = 9): (A) first heating of the noncrystalline sample at 20 °C/min; (B) first cooling with −10 °C/min; (C) second cooling with −20 °C/min; (D) third cooling with −40 °C/min; (E) fourth cooling with −80 °C/min; (F) second heating after annealing at 130 °C.

conducted at a heating and cooling rate of 20 °C/min revealed a glass-transition step and one strong exotherm in the cooling curve. The enthalpies of these phase transitions (see Table 2) indicate transitions between the isotropic melt and either a smectic liquid crystalline (LC) phase or a crystalline phase. When the cooling rate was varied between −10 and −80 °C/min, the exotherm exhibited only a moderate temperature shift (over a range of 10−15 °C) (Figure 2). This slight temperature dependence is a good indicator of the formation of an LC phase upon cooling.

Optical microscopy with crossed polarizers revealed an isotropic phase above the endotherm. The birefringent phase formed at the temperature of the exotherm upon cooling was in all three cases highly viscous and difficult to shear. However, in the case of **2e** the LC phase was mobile enough to allow slow shearing between glass plates. The texture may be described as a kind of "schlieren texture", but without the black threads of a typical nematic schlieren texture. The battonet or fan-shaped texture which was reported for other polyimides[5,7] was never detectable in the case of **2b, 2d,** or **2e**. These observations point toward a smectic-C phase.

WAXD powder patterns of PEI's **2a,c,e** were recorded after cooling from the isotropic melt in air, without
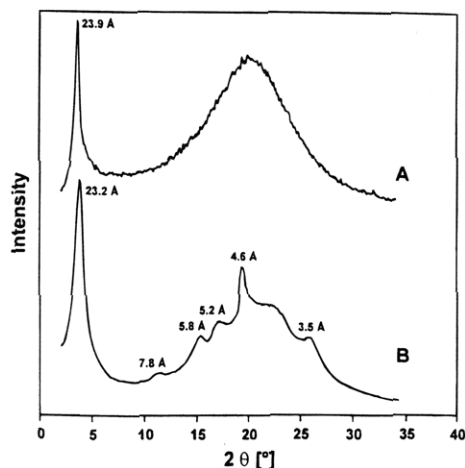
Figure 3. WAXD powder patterns of poly(ester–imide) **2e**: (A) after rapid cooling from the isotropic melt; (B) after annealing at 140 °C for 24 h.
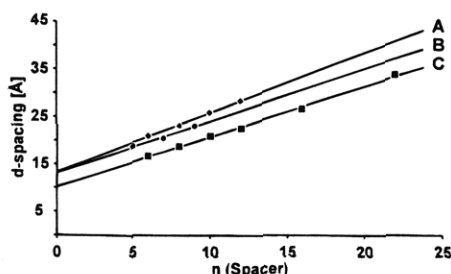

Figure 4. Plot of *d*-spacings of the PEI's **2a–i** versus the number of CH₂ groups in the spacers. The *d*-spacings were calculated from the middle-angle reflections of glassy **2a,c,e** (B), from glassy **2b,d,f,g** (A), and from crystalline (annealed) **2b,d,f,g,h,i** (C).

Figure 5. MAXD powder pattern of PEI **2e** recorded with synchrotron radiation at a heating and cooling rate of 20 °C/min.

Figure 6. X-ray fiber pattern of (A) PEI **2e** and (B) its schematic interpretation according to ref 11.

annealing. As illustrated by Figure 3A, these WAXD patterns do not display any wide-angle reflection, but a sharp middle-angle reflection (MAR). This result allows the following conclusions. The PEI's form a smectic layer structure, without any order of the mesogens inside their layers. In other words, they form a smectic glass below T_g, in agreement with the pronounced glass-transition step in the DSC curves. The absence of any wide-angle reflection also means that the melt above T_g is a smectic-A or smectic-C phase. In the case of **2e** annealing above T_g (e.g., at 120 or 140 °C) induced partial crystallization (Figure 3B). In contrast, **2a** and **2c** were reluctant to crystallization even upon annealing. Obviously, longer spacers favor the crystallization from a kinetic point of view. The same structure–property relationship was been found for the PEI's of structure **1**[9] containing odd spacers, but a positive influence of the longer alkylene spacer on the crystallization kinetic is also known from poly(butylene terephthalate) when compared to poly(ethylene terephthalate).

Calculation of the layer distances (*d*-spacings) from the MAR's yielded the values plotted as line "B" in Figure 4. Extrapolation of line "B" toward zero CH₂ groups of the spacer yielded a virtual length of the mesogenic unit around 13 Å. The theoretical value calculated for a fully extended mesogen by means of a force-field program amounts to 15.0 Å from CO to CO or to 17.7–18.0 Å including both oxygens of the diol spacer and one additional σ-bond. Thus the comparison of the extrapolated and of the calculated value clearly indicates a tilting of the mesogen relative to the layer planes. Thus it may be concluded that the smectic phase above T_g is a smectic-C phase, in good agreement
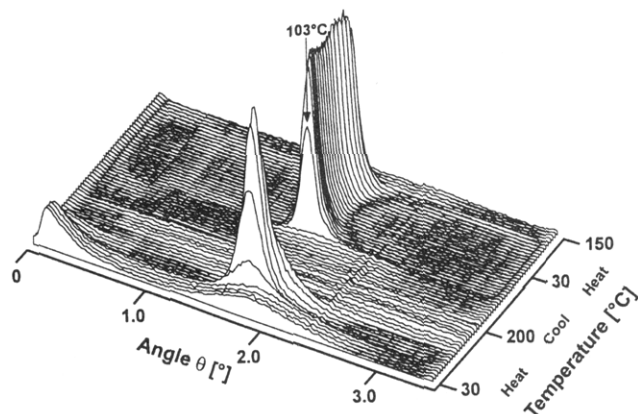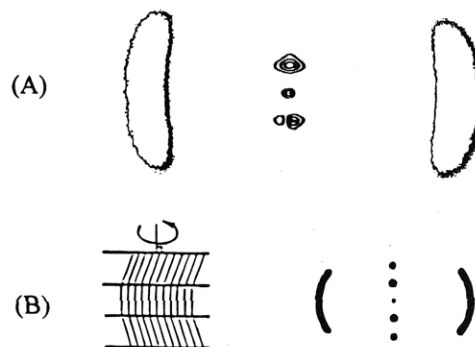
with their texture and high viscosity. The identification of the smectic LC phase on the basis of WAXD powder patterns recorded at 20 °C is, of course, only correct when the *d*-spacing does not change upon cooling (or heating). In order to check this point, middle-angle X-ray diffraction patterns (MAXD) of **2e** were recorded with synchrotron radiation at a heating and cooling rate of 10 °C/min. As demonstrated by Figure 5, the MAR vanishes at the temperature of the DSC endotherm and reappears along with the exotherm without changing its position. This result clearly confirms the above interpretation.

Furthermore, fiber patterns of the frozen LC phase of PEI **2e** (*n* = 9) and of PEI **2g** (*n* = 12) were recorded. In the case of **2e** (Figure 6), the expected halo appears on the equator and sharp layer reflections exactly on the meridian. Thus, this fiber pattern does not carry more information than the corresponding powder pattern. There is not direct evidence for the tilting of the mesogens. Nonetheless, this fiber pattern does not disagree with the existence of a frozen smectic-C phase, because it may happen that the direction of the tilt (at constant tilt angle!) is azimuthally disordered in subsegment layers as schematically illustrated in Figure 6B. In contrast, the fiber pattern of **2g** displays four maxima off the meridian ($\beta = 30°$), in agreement with the tilted structure outlined in Figure 7. Thus, the fiber pattern of **2g** proves that the frozen LC phase has a smectic-C structure. Such fiber patterns and their interpretation were published by Leadbetter and Norrish,[11] so a more detailed discussion is not required here.

Properties of PEI'ss with Even Spacers. When DSC measurements of the PEI's **2b,d,f,g,h,i** (the "even PEI's") were conducted, a glass-transition step and one endotherm (T_m in Table 2) were detectable in the
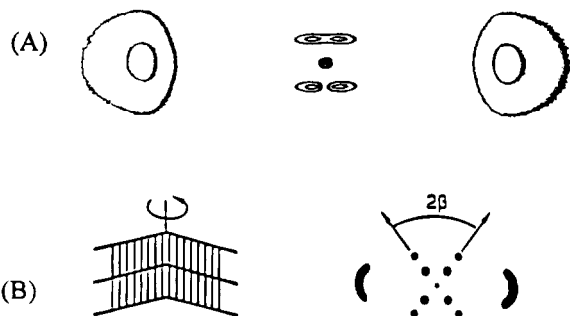
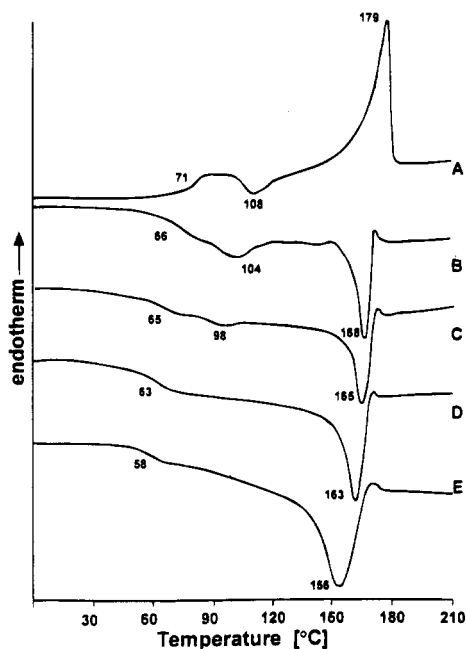**Figure 7.** X-ray fiber pattern of (A) PEI **2g** and (B) its schematic interpretation according to ref 11.

Figure 8. DSC measurements of PEI **2f**: (A) first heating after annealing at 140 °C; (B) first cooling with −10 °C/min; (C) cooling with −20 °C/min; (D) cooling with −40 °C/min; (E) cooling with −80 °C/min.

heating curve (Figures 6 and 7) quite analogous to **2a,c,e**. Furthermore, the melt formed above this endotherm is isotropic as revealed by optical microscopy (T_i in Table 2). However, a more complex pattern of thermal properties become detectable upon cooling.

The DSC cooling curves of all even PEI's display two exotherms, indicating the formation of a monotropic LC phase. Therefore, the cooling rate was varied between −10 and −80 °C/min. As illustrated by Figures 8 and 9, the high-temperature exotherm depends relatively little on the rate of cooling. In agreement with the microscopic observations, this exotherm represents the formation of a smectic LC phase from the isotropic melt (anisotropization). The texture and the high viscosity of this LC phase is similar to that of the odd PEI's.

The low-temperature exotherm represents the crystallization (T_c in Table 2). Correspondingly, its temperature depends very much on the cooling rate (Figures 8 and 9). The rate of crystallization depends in turn considerably on the length of the spacer. This dependence is clearly detectable even when two directly neighboring even PEI's such as **2f** and **2g** are compared (Figures 8 and 9). In the case of **2f**, a cooling rate > −20 °C/min results in a freezing in of the LC phase, whereas in the case of **2g** even cooling with −80 °C/min does not suppress the crystallization. Yet quenching from the
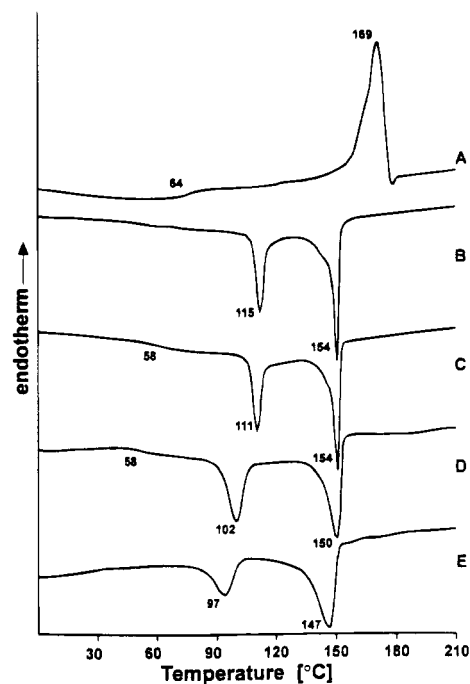

Figure 9. DSC measurements of PEI **2g**: (A) first heating after annealing at 240 °C; (B) first cooling with −10 °C/min; (C) cooling with −20 °C/min; (D) cooling with −40 °C/min; (E) cooling with −80 °C/min.
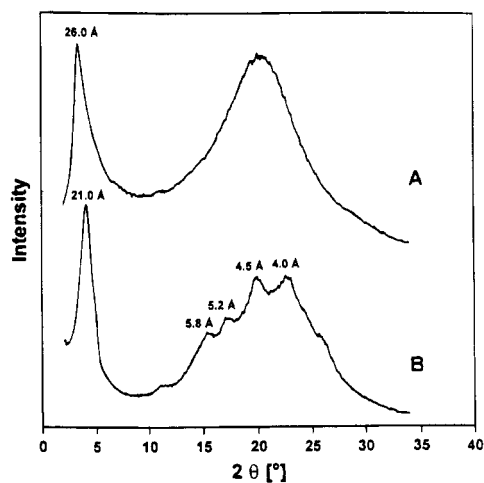

Figure 10. WAXD powder patterns of PEI **2f**: (A) after quenching from the isotropic melt; (B) after annealing at 140 °C.

isotropic melt (190 °C) with ice also suppressed the crystallization of **2g** (Figure 10). In other words, it was feasible to suppress the crystallization of **2b,d,f,g** and to freeze in their smectic LC phases. However, in the case of **2h** and **2i**, the rate of crystallization is so high that quenching with ice or methanol/CO_2 did not completely prevent their crystallization.

The WAXD powder patterns of all even PEI's were recorded after annealing at 140 °C to make sure that the crystalline phase was measured. The resulting WAXD patterns were nearly identical, so that Figure 10B is representative for WAXD patterns of all crystalline even PEI's. The wide-angle reflections exclude a hexagonal arrangement of the mesogens and thus suggest a kind of orthorhombic (smectic-E like) or monoclinic (smectic-H like) array. The presence of a strong MAR indicates the existence of a layer structure in all cases. The layer distances of calculated from these MARs via the Bragg equation are listed in Table 3 and

Table 3. Layer Distances (*d*-Spacings) As Determined from the Middle-Angle Reflections via the Bragg Equation

polymer formula	*d*-spacings		polymer formula	*d*-spacings	
	quenched[a]	annealed[b]		quenched[a]	annealed[b]
2a		18.8	**2f**	26.0	21.0
2b	21.0	16.7	**2g**	28.5	23.6
2c	20.5	20.5	**2h**	26.7	26.7
2d	23.2	18.8	**2i**	33.9	33.9

[a] Quenched from the isotropic melt at 180–200 °C with ice. [b] Annealed at 135 or 140 °C for 24 h.
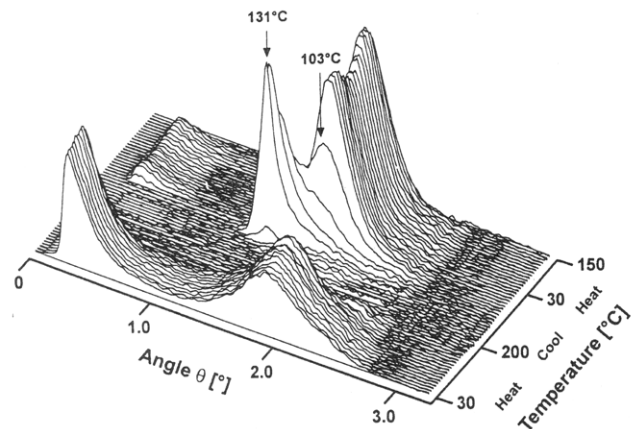
Figure 11. MAXD measurements of PEI **2g** with synchrotron radiation at a heating and cooling rate of 20 °C/min.

plotted versus the lengths of the spacers in Figure 4 (line C). They fall on a straight line with a slope of 1.06 Å per CH₂ group, which is halfway in between the "pitch" of an all-gauche (0.90 Å) and the "pitch" of an all-trans (1.27 Å) alkane chain. It is almost identical with the value calculated from the MARs of the odd spacers, which amounts to 1.10 Å per CH₂ group (line B in Figure 4).

In the case of PEI's **2b,d,f,g**, the WAXD powder patterns of the quenched LC phase display again a strong MAR, but no additional reflections. Figure 10A is a representative example for all these WAXD patterns. Such WAXD patterns are typical for a frozen smectic-A or -C phase quite analogous to that of the "odd PEI's". The *d*-spacings calculated from these MARs fall again on a straight line (line A in Figure 4), but the slope is now greater (1.24 Å/CH₂) so that it comes close to that of an all-trans alkane chain. This suggest at first glance that the smectic LC phase contains a significantly higher fraction of trans conformation than the crystalline phase.

Another interesting result was obtained by extrapolation of the layer distances toward zero CH₂ groups. In the case of the frozen LC phase, a *d*-spacing of 13.0 Å was obtained, indicating a considerable tilting of the mesogenic unit quite analogous to the LC phase of the odd PEI's. This result is in perfect agreement with the fiber pattern of **2g** (Figure 7) discussed above. A much smaller value, namely, 10.5 Å, was found for the crystalline state of the even PEI's. This means that the mesogens are much more tilted in the crystalline state corresponding to the order of a smectic-H phase. This interpretation of the WAXD patterns recorded at 25 °C was confirmed by synchrotron radiation measurements of PEI **2g** conducted at a heating and cooling rate of 10 °C/min. Figure 11 clearly demonstrates that the MAR of the molten **2g** shifts to a wider angle and thus to a shorter layer distance upon crystallization. Thus, the

temperature-dependent MAXD measurements perfectly agree with a smectic-C/crystalline smectic-H transition, but with a stronger tilt in the solid phase. In this connection, we wish to point out that the term "crystalline smectic-H" means a greater long-range order of the mesogens in the chain direction as compared to a typical smectic-H mesophase of low molar mass LC compounds. However, a clear-cut borderline between a conformational disordered crystallite with a smectic-H type layer structure and a smectic-H mesophase does not exist. It should be emphasized that the results presented here do not allow a detailed description of the crystalline phase of the even-numbered PEI's. However, a smectic-H like layer structure is evident.

Finally, the transition enthalpies listed in Table 2 need a short comment. The endotherms of the even PEI's include a much higher enthalpy change than those of the odd PEI's because they include the melting enthalpy of the crystalline smectic-H phase. Another interesting trend is the steep increase of the crystallization enthalpy with increasing lengths of the spacers. This trend is directly evident from the exotherms in the cooling traces of **2f** and **2g** in Figures 8 and 9. As mentioned above, the longer spacers favor a higher rate of crystallization, and at a fixed time interval the PEI's with long spacers obviously reach a higher degree of crystallization. This conclusion is confirmed by a direct comparison of the WAXD patterns of **2b** or **2d** with those of **2h** or **2i**, when all samples were annealed under identical conditions. It is a reasonable assumption that the change of the tilt angle and the rotational ordering inside the layers of the mesogens are favored by the higher mobility of the longer spacers. A further contribution may come from the formation of ordered paraffin domains discussed below.

Formation of Paraffin Domains. From rigid-rod polymers (e.g., polyester, polyaramides, poly(benzobisoxazoles)) containing laterally attached *n*-alkyl substituents it is known that they form sanidic layer structures.[11-16] The *n*-alkyl chains which are located between the stacks of the main chains can form ordered paraffin domains. The chain segments involved in these paraffin domains adopt the all-trans conformation and form either a disordered hexagonal array or, if long enough, a crystalline phase. Hence the question arises, are long aliphatic spacers in smectic systems also capable of forming ordered paraffin domains?

The existence of ordered paraffin domains built up by chain segments in all-trans conformation should be detectable by ¹³C NMR CP/MAS spectroscopy. It is well known from semicrystalline polyethylene and from the *n*-alkyl-substituted rigid-rod polymers that the gauche and trans conformations yield CH₂ signals of different chemical shifts (tg 30–31 and tt 33–34 ppm, respectively), if no rapid exchange ($V_{ex} > 2.2\delta v$) between both conformations takes place.

Therefore, the three PEI's with the longest spacers, **2g,h,i**, were examined by ¹³C NMR CP/MAS spectroscopy at 25 and 100 °C. The spectra, summarized in Figure 12, display in all cases a strong broad peak around 30 ppm representing the gauche conformations of disordered more or less mobile chain segments. In the case of **2g**, a shoulder is detectable at 32–33 ppm, which vanishes at 100 °C and presumably indicates the presence of rather stable all-trans conformations. In the case of **2h** and **2i**, a relatively sharp peak appears at 33 ppm, the intensity of which decreases at 100 °C. This peak obviously represents the existence of all-trans
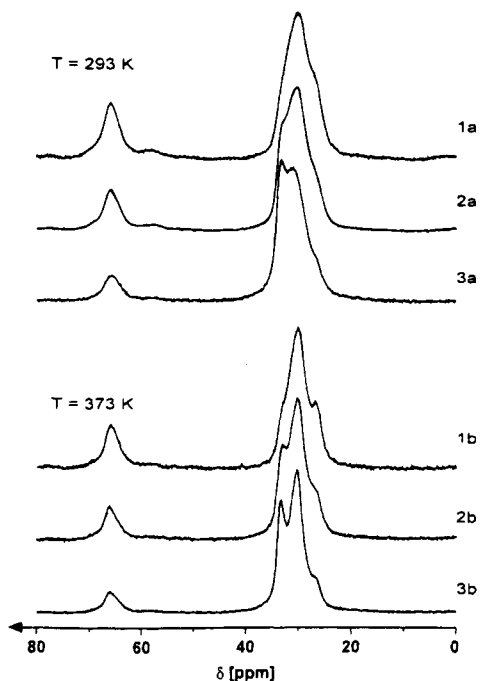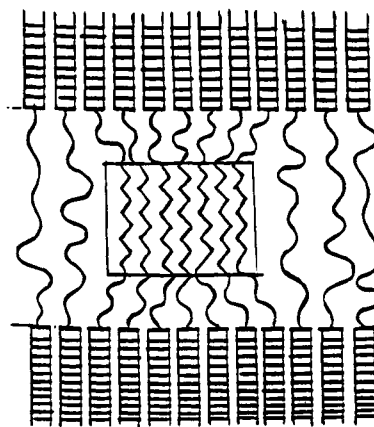
Figure 12. 75.4 MHz ^{13}C NMR CP/MAS spectra of the poly-(ester–imide)s **2g** (1a), **2h** (2a, 2b), and **2i** (3a, 3b).

Figure 13. Schematic illustration of an ordered paraffin domain formed by long alkylene spacers between the "two-dimensional" crystals of the mesogens.

chain segments in relatively thermostable paraffin domains. The existence of such domains even at 100 °C results from the fact that the spacers are attached with both ends to the immobile mesogens. In the case of the sanidic structures, the alkyl side chains are only fixed at one end, and the paraffin domains of *n*-hexadecyl groups show then a melting temperature in the range of 60–75 °C.$^{12-17}$ Thus, the above interpretation of the ^{13}C NMR spectra of **2g,h,i** is in reasonable agreement with the well-documented properties of sanidic layer systems.

Since the alkyl chains in all-trans conformation possess a smaller cross section than the imide mesogens, the formation of paraffin domains should create free volume in their neighborhood and result in a contraction of the layer distances compared to a situation with fully extended spacers: A schematic illustration of a paraffin domain embedded between layers of mesogens is given in Figure 13. The assumption of a contraction of the layer distances despite a high fraction of trans conformation agrees in turn with the measured *d*-spacings, which clearly show that the average pitch of a CH_2CH_2 unit (2.14 Å) is smaller than the 2.54 Å expected for a fully extended all-trans chain. A more detailed study of such smectic paraffin systems including ^{2}H NMR measurements is given in a separate paper dealing with PEI's of structure **1**.

Conclusion

The results of this study allow the following conclusions. The PEI's of structure **2** are semicrystalline polymers which form monotropic LC phases upon cooling. The rate of crystallization decreases with shorter spacers and is particularly low for the odd-numbered

spacers. All PEI's of structure **2** form a layer structure in all solid and anisotropic liquid phases, with the mesogens tilted relative to the layer plane. In other words, the LC phase has a smectic-C character. This property is quite unusual, because most thermotropic poly(ester–imide)s, poly(ether–imide)s, and poly(amide–imide)s reported so far form a smectic-A phase or in rare cases a nematic melt. Another interesting result is the finding that the long alkane spacers tend to form ordered paraffin domains between the layers of the mesogens. Studies of the photoreactivity will be described in a future publication.

References and Notes

(1) Kricheldorf, H. R. *Mol. Cryst. Liq. Cryst.* **1994**, *254*, 87.
(2) Karayanmidis, G.; Standos, D.; Bikiaridis, D. *Makromol. Chem.* **1993**, *194*, 1209.
(3) Pardey, R.; Shen, D.; Gabori, P. A.; Harris, F. W.; Cheng, S. Z. D.; Aducci, J.; Facinelli, J. V.; Lenz, R. W. *Macromolecules* **1993**, *26*, 3687.
(4) Pardey, R.; Wa, S. S.; Chen, J.; Harris, F. W.; Cheng, S. Z. D.; Keller, A.; Aducci, J.; Facinelli, J. V.; Lenz, R. .W. *Macromolecules* **1994**, *27*, 5794.
(5) Abajo, J. de; Campa, J. de la; Kricheldorf, H. R.; Schwarz, G. *Polymer* **1994**, *35*, 7.
(6) Kricheldorf, H. R.; Schwarz, G.; Berghahn, M.; Abajo, J. de; Campa, J. de la *Macromolecules* **1994**, *27*, 2540.
(7) Kricheldorf, H. R.; Linzer, V. *J. Polym. Sci., Part A: Polym. Chem.*, in press (LC-Polyimides 19).
(8) Kricheldorf, H. R.; Gurau, M. *J. Polym. Sci., Part A: Polym. Chem.*, in press (LC-Polyimides 21).
(9) Kricheldorf, H. R.; Schwarz, G.; Abajo, J. de; Campa, J. de la *Polymer* **1991**, *32*, 942.
(10) Kricheldorf, H. R.; Berghahn, M.; Gurau, M.; Probst, N. *Macromolecules*, submitted (LC-Polyimides 20).
(11) Leadbetter, A. J.; Norrish, E. K. *Mol. Phys.* **1979**, *38*, 669.
(12) Ballauff, M. *Angew. Chem.* **1989**, *101*, 261.
(13) Stern, R.; Ballauff, M.; Lieser, G.; Wegner, G. *Polymer* **1991**, *32*, 2096.
(14) Wittaker, A. K.; Falk, U.; Spiess, H. W. *Makromol. Chem.* **1989**, *190*, 1603.
(15) Biswas, A.; Deutscher, K.; Blackwell, J.; Wegner, G. *Polym. Prepr. (Am. Chem. Soc., Div. Polym. Chem.)* **1992**, *37* (1), 286.
(16) Clauss, J.; Schmidt-Rohr, K.; Adam, A.; Boeffel, C.; Spiess, H. W. *Macromolecules* **1992**, *25*, 5208.
(17) Kricheldorf, H. R.; Domschke, A. *Macromolecules* **1994**, *27*, 1509.